Transverse Mode-Encoded Quantum Gate on a Silicon Photonic Chip

Lan-Tian Feng,[1,2,*] Ming Zhang,[3,4,*] Xiao Xiong,[1,2] Di Liu,[1,2] Yu-Jie Cheng,[1,2] Fang-Ming Jing,[1,2] Xiao-Zhuo Qi,[1,2] Yang Chen,[1,2] De-Yong He,[1,2] Guo-Ping Guo,[1,2] Guang-Can Guo,[1,2] Dao-Xin Dai,[3,4,†] and Xi-Feng Ren[1,2,‡]

[1]*Key Laboratory of Quantum Information, CAS, University of Science and Technology of China, Hefei 230026, China*
[2]*Synergetic Innovation Center of Quantum Information & Quantum Physics, University of Science and Technology of China, Hefei 230026, China*
[3]*State Key Laboratory for Modern Optical Instrumentation, Centre for Optical and Electromagnetic Research, Zhejiang Provincial Key Laboratory for Sensing Technologies, Zhejiang University, Zijingang Campus, Hangzhou 310058, China*
[4]*Ningbo Research Institute, Zhejiang University, Ningbo 315100, China*

(Received 19 April 2021; accepted 25 January 2022; published 10 February 2022)

As an important degree of freedom (d.o.f.) in photonic integrated circuits, the orthogonal transverse mode provides a promising and flexible way to increase communication capability, for both classical and quantum information processing. To construct large-scale on-chip multimode multi-d.o.f.s quantum systems, a transverse mode-encoded controlled-NOT (CNOT) gate is necessary. Here, with the help of our new transverse mode-dependent directional coupler and attenuator, we demonstrate the first multimode implementation of a 2-qubit quantum gate. The ability of the gate is demonstrated by entangling two separated transverse mode qubits with an average fidelity of 0.89 ± 0.02 and the achievement of 10 standard deviations of violations in the quantum nonlocality verification. In addition, a fidelity of 0.82 ± 0.01 is obtained from quantum process tomography used to completely characterize the CNOT gate. Our work paves the way for universal transverse mode-encoded quantum operations and large-scale multimode multi-d.o.f.s quantum systems.

DOI: 10.1103/PhysRevLett.128.060501

In integrated photonics, the significant enhancement of information processing and communication capability is an ultimate goal due to the exponential growth in the demands of optical interconnects and communication for both classical [1] and quantum [2] information applications. To achieve large-scale photonic quantum systems, multiphoton, multiple degrees of freedom (d.o.f.s) and high-dimensional encoding are becoming attractive and essential [3]. In recent years, a lot of experimental efforts to achieve universal quantum operations have been done with different d.o.f.s, such as a single qubit operation and 2-qubit controlled-NOT (CNOT) gate with path or polarization encoding [4–9], as well as a 2-qubit quantum gate for time-bin qubits [10,11] and frequency-bin qubits [12]. In addition, hybrid encoding with multiple d.o.f.s has also shown impressive applications such as superdense coding [13] and multi-d.o.f.s teleportation [14].

More recently, the orthogonal transverse modes supported in a multimode waveguide are valued and developed rapidly for their high-dimensional scalability, compactness, and coherent conversion with other d.o.f.s [15–18]. As a new d.o.f., the transverse mode provides the flexibility and scalability for a wide scope of novel applications, such as dense optical interconnects [1,16,17], quantum information science [18–21], nonlinear photonics [22,23], and so on. Specifically, one single waveguide can support ten channels simultaneously by multiplexing transverse modes [17], thus, greatly improving the scalability. Using intermode spontaneous nonlinear processes, an integrated near-ideal spontaneous photon source [21] and high-efficiency second harmonic generation [22] can also be achieved. Meanwhile, a variety of multimode photonic devices such as mode (de) multiplexers [24,25], grating couplers [26], switches [27–29], filters [30], sharp waveguide bends and mode-independent crossings [31,32], and many other building blocks [33] have been developed intensively in recent years. However, as a potential on-chip d.o.f., the full manipulation of transverse mode qubits, especially a 2-qubit CNOT gate, is still not studied extensively and is challenging.

In this Letter, we report the on-chip generation, manipulation, and measurement of transverse mode-encoded quantum entangled states based on a compact CNOT gate. The CNOT gate relies on two newly developed multimode photonic devices that can selectively manipulate different transverse modes, called the unbalanced transverse mode-dependent directional coupler (TMDDC) and multimode attenuator (MMA). This multimode waveguide CNOT gate is very compact and has a size of $\sim 10 \times 160\ \mu m^2$. We characterize it by performing quantum state tomography and quantum process tomography measurements. The gate realizes the entanglement of 2 separable qubits with an average state fidelity of $\bar{F}_s = 0.89 \pm 0.02$ and a process

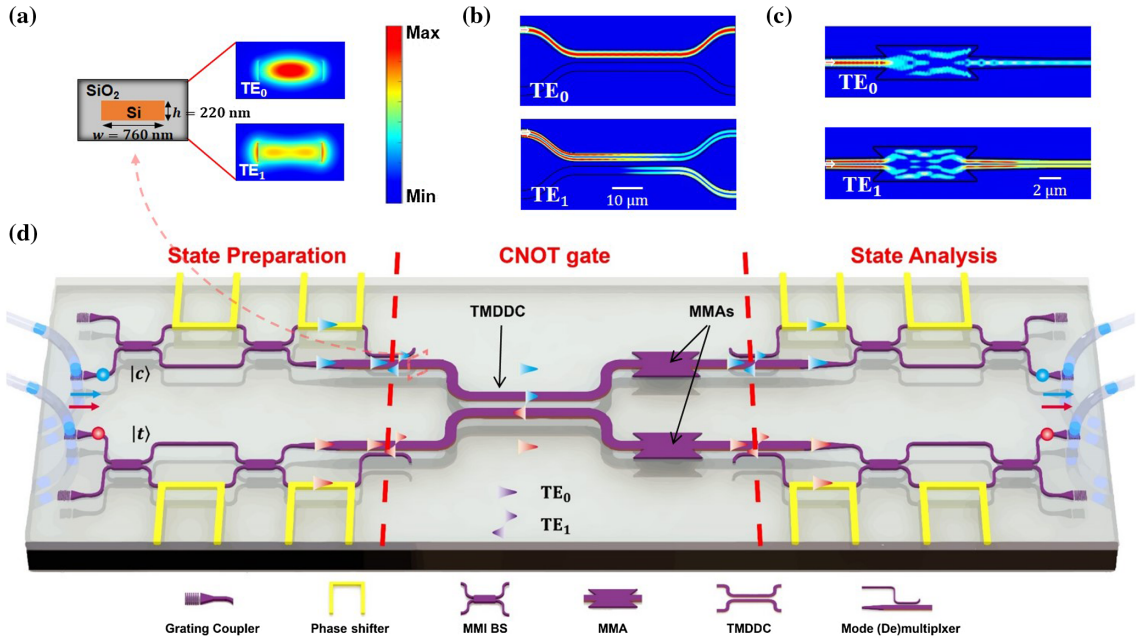

FIG. 1. Transverse mode-encoded quantum CNOT gate and the entire circuit. (a) The transverse modes in a multimode photonic waveguide. Min and max in scale bar represent the relative energy density. (b) Simulated light propagation in the designed transverse mode-dependent directional coupler. (c) Simulated light propagation in the designed multimode attenuator. (d) Schematic of the entire silicon photonic integrated circuit. The red dashed lines mark out the multimode section, where both modes are supported and function together as a transverse mode-encoded CNOT gate. The other parts of the circuits are single-mode and used for the state preparation and analysis. MMI BS: multimode interference beam splitter.

fidelity of $F_p = 0.82 \pm 0.01$. Because the transverse mode-encoding is compatible with other encoding protocols and facilitates the construction of quantum photonic integrated circuits (QPICs) with higher dimensions and capacity, our work paves the way for universal transverse mode-encoded quantum operations and practical applications in compact and scalable photonic quantum processing with multiple d.o.f.s.

A quantum processor requires a cascade of various unitary operations, which consist of a finite series of basic logic gates. It has been proven that the 2-qubit CNOT gate, which flips the target qubit $|t\rangle$ depending on the state of the control qubit $|c\rangle$, together with single-qubit logic gates, are sufficient for a universal quantum operation [34]. In QPICs, the universal quantum operation is often implemented using beam splitters and phase controllers [4,7–9]. The 2-qubit CNOT gate is mainly composed of three unbalanced directional couplers [8], one for two-photon interaction by the Hong-Ou-Mandel effect [35], and the other two for energy compensation.

Among various material systems for QPICs, silicon on insulator is chosen here because of its excellent optical properties and complementary metal-oxide-semiconductor compatibility [36]. The designed multimode waveguide has a cross section of 760×220 nm^2 and supports the two lowest-order transverse modes of TE polarization, i.e., the TE_0 and TE_1 modes, as shown in Fig. 1(a). These modes are orthogonal to each other and without cross-coupling they can be directly used for quantum information encoding. To achieve a transverse mode-encoded CNOT gate, we have two newly designed mode-dependent photonic devices, TMDDC and MMA, which can achieve mode-dependent coupling and loss, as shown in Figs. 1(b) and 1(c), respectively. By cascading one TMDDC and two MMAs, a multimode 2-qubit CNOT gate is constructed, as shown in Fig. 1(d).

The present TMMDC is based on a symmetric directional coupler, in which the incident modes (i.e., TE_0, TE_1) are partially transferred to the adjacent waveguide through the evanescent coupling. Here, to achieve a mode-selective beam splitter, we choose a wide waveguide with a core width of $w_0 = 760$ nm and a large gap of $g = 400$ nm. In this situation, the evanescent field of the TE_0 mode is restricted strongly in the waveguide core, and there is rarely power transfer. In contrast, the TE_1 mode has sufficient coupling strength, and the coupling length is chosen as $L = 32.5$ μm to realize a cross-coupling ratio of 2/3. Fig. 1(b) shows the simulated light propagation in the designed structure when the TE_0 and TE_1 modes are launched, respectively. The MMA is designed to attenuate 2/3 power of the TE_0 mode and guarantee lossless propagation of the TE_1 mode for energy compensation. In order to realize such an energy attenuator, a multimode interferometer (MMI) is introduced because of its compactness ($< 3 \times 10$ μm^2) and low insertion losses (< 0.5 dB). For the lossless propagation of the TE_1 mode, we choose the MMI length to form

the self-imaging for the TE_1 mode. In this case, the TE_0 mode shows imperfect self-imaging, and the output energy depends on the waveguide width. Here, we choose the MMI width as $w = 2.5\ \mu$m and the MMI length as $l = 7.5\ \mu$m. With this design, one can maintain the lossless propagation for the TE_1 mode while attenuating 2/3 of the power of the TE_0 mode. In order to radiate away the unwanted energy left in the attenuator, which would cause unnecessary interference and negatively affect the output, we introduce a butterfly-shaped MMI section to reduce the reflection of the TE_0 mode by introducing four acute angles to the MMI section. Figure 1(c) shows the simulated light propagation in the designed attenuator when the TE_0 and TE_1 modes are launched, respectively. For more information on these two devices, please see the Supplemental Material, Sec. I [37]. The function of controlling the transverse modes separately here enables us to further cascade them for realizing complex functions with mode encoding such as a 2-qubit CNOT gate.

A PPKTP crystal was used to generate frequency-degenerate photon pairs centered at a wavelength of 1540 nm. More details are provided in the Supplemental Material, Sec. II [37]. The photon pairs were collected with a single-mode fiber array and then coupled into the TE_0 mode in the on-chip single-mode waveguides via grating couplers. To encode photons with different transverse modes, mode (de)multiplexers [1] were introduced before (after) the photons which have passed through the CNOT gate. After the on-chip state evolution, the photons were coupled by using another fiber array and detected with superconducting single-photon detectors. To prepare and detect different quantum states, path-encoding Mach-Zehnder interferometers (MZIs) were performed. Microheaters controlled by a homemade multichannel direct-current regulated power supply were used to thermally tune the phases of the photons. All the heaters were individually characterized and displayed high quality. For further details, please see the Supplemental Material, Sec. IV [37].

To characterize the chip with different input qubits, we defined logical and physical qubits with the following states: $|0\rangle_c = |\mathrm{TE}_0\rangle$, $|1\rangle_c = |\mathrm{TE}_1\rangle$, $|0\rangle_t = (|\mathrm{TE}_0\rangle + |\mathrm{TE}_1\rangle)/\sqrt{2}$, $|1\rangle_t = (|\mathrm{TE}_0\rangle - |\mathrm{TE}_1\rangle)/\sqrt{2}$, where the subscripts c and t denote the control and target qubits. The CNOT gate has a success probability of $P = 1/9$, which can be rendered deterministic by making use of ancillary resources, measurements, and feed forward [38].

Two-photon quantum interference is essential in the CNOT gate, and the gate operation succeeds when two photons arrive at the directional coupler at the same time; thus, the performance of the CNOT gate is directly related to the interference visibility. We first characterized the quantum interference in the multimode directional coupler. The interference results are shown in Fig. 2. An interference visibility of 0.82 ± 0.03 was derived from Gaussian fitting before background subtraction (the raw data used, the same below) where the error was the fitting standard error. Here, the visibility is defined as $V = (C_{\max} - C_{\min})/C_{\max}$, where $C_{\max}$ and $C_{\min}$ are the maximum and minimum of fitted data, respectively. The visibility is very close to the ideal value of 0.80 [6], which is indicated by the dashed blue line in Fig. 2. The excellent agreement between the measured and ideal cases proves that the TMDDC works well. The CNOT gate operation will be realized at zero time delay (dip position).

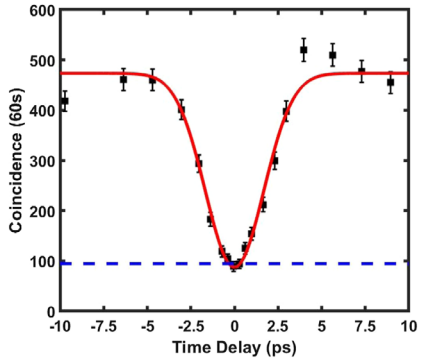

FIG. 2. Quantum interference in the transverse mode-dependent directional coupler. Both the control and target photons are in the TE_1 mode and have an adjustable time delay between them. The dashed blue line denotes the lower limit for the ideal case. The error bars represent $\pm\sqrt{N}$ for the raw coincidence data (black rectangles) N. The dots denote the experimental data, and the curve is the corresponding Gaussian fit.

The basic function of a CNOT gate is entangling 2 separate qubits, which is one fundamental operation in quantum information processing. With a perfect CNOT gate and taking one of the states $\{|\pm\rangle_c|0\rangle_t, |\pm\rangle_c|1\rangle_t\}$ where $|+\rangle_c = (|0\rangle_c + |1\rangle_c)/\sqrt{2}$ and $|-\rangle_c = (|0\rangle_c - |1\rangle_c)/\sqrt{2}$ as input, the output state is expected to be the maximally entangled Bell state, that is,

$$|\Phi^{\pm}\rangle = \frac{1}{\sqrt{2}}(|0\rangle_c|0\rangle_t \pm |1\rangle_c|1\rangle_t),$$
$$|\Psi^{\pm}\rangle = \frac{1}{\sqrt{2}}(|0\rangle_c|1\rangle_t \pm |1\rangle_c|0\rangle_t). \quad (1)$$

The corresponding density matrix is denoted as $\hat{\rho}_{\mathrm{ideal}} = |\phi\rangle\langle\phi|$, where $|\phi\rangle = |\Phi^{\pm}\rangle, |\Psi^{\pm}\rangle$. We reconstructed the density matrix of the output quantum state by quantum state tomography [39]. Figure 3 shows the real parts of the reconstructed density matrices $\hat{\rho}_{\mathrm{mea}}$ and $\hat{\rho}_{\mathrm{ideal}}$ (crystal clear bars). The raw fidelity of the generated state, defined as $F_s = [\mathrm{Tr}(\sqrt{\sqrt{\hat{\rho}_{\mathrm{mea}}}\hat{\rho}_{\mathrm{ideal}}\sqrt{\hat{\rho}_{\mathrm{mea}}}})]^2$, were calculated for the different output states as $F_{|\Phi^+\rangle} = 0.89 \pm 0.03$, $F_{|\Phi^-\rangle} = 0.88 \pm 0.03$, $F_{|\Psi^+\rangle} = 0.90 \pm 0.02$, $F_{|\Psi^-\rangle} = 0.87 \pm 0.02$. The averaged fidelity was obtained as $\bar{F}_s = 0.89 \pm 0.02$, which confirms the entangling function of the CNOT gate. The fidelity errors were obtained by a 100-times Monto

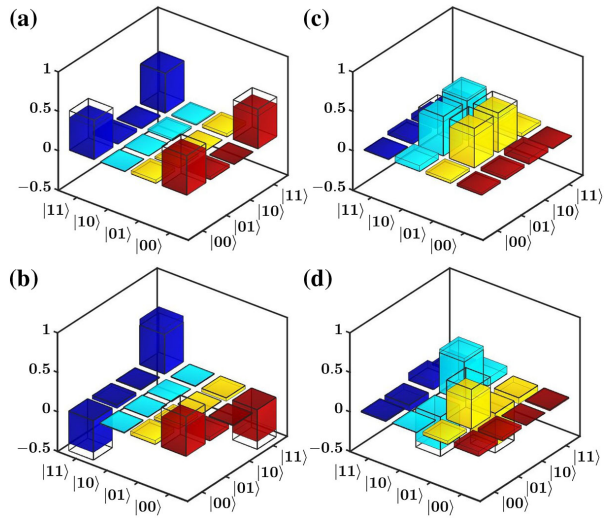

FIG. 3. Quantum state tomography of the generated Bell states. The real parts of the measured density matrices of the output states with the different input states of (a) $|+\rangle_c|0\rangle_t$, (b) $|-\rangle_c|0\rangle_t$, (c) $|+\rangle_c|1\rangle_t$, and (d) $|-\rangle_c|1\rangle_t$. The imaginary parts of the measured density matrices are negligible. The clear bars represent the ideal density matrices for the maximally entangled Bell states $|\Phi^{\pm}\rangle$ and $|\Psi^{\pm}\rangle$.

Carlo calculation with the experimental data subjected to Gaussian statistics. In addition, the linear entropy and tangle were calculated to quantify the mixture and amount of entanglement for these states [39–41]. The details are provided in the Supplemental Material, Sec. V [37].

The nonlocality nature of the output states was further verified using the Clauser-Horne-Shimony-Holt inequality [42],

$$\hat{S}(\hat{\rho}) = E(a,b) - E(a,b') + E(a',b) + E(a',b'). \quad (2)$$

Here, a, a' and b, b' are two sets of measurement direction settings for different qubits. For a state that can be described by a local classical theory, the nonlocality parameter $\hat{S}$ should be less than or equal to 2. For entangled Bell states, quantum mechanics predicts a maximal value of $\hat{S}_{\max} = 2\sqrt{2}$ with a selected measurement basis. In this study, the phases in the MZIs at the measuring part were individually set as $\{0°, 180°, 45°, 225°\}$ for the control qubit and $\{22.5°, 202.5°, 67.5°, 247.5°\}$ for the target qubit. In this way, $\hat{S}$ values for the different output states were obtained as $\hat{S}_{|\Phi^+\rangle} = 2.54 \pm 0.05$, $\hat{S}_{|\Phi^-\rangle} = 2.50 \pm 0.05$, $\hat{S}_{|\Psi^+\rangle} = 2.51 \pm 0.05$, $\hat{S}_{|\Psi^+\rangle} = 2.43 \pm 0.05$. The average value is $\hat{S}_{\text{Bell}} = 2.50 \pm 0.05$, which violates the inequality by 10 standard deviations.

Finally, we performed quantum process tomography to fully characterize the quantum device. We prepared 16 different input states from the set $\{|0\rangle, |1\rangle, |0\rangle + |1\rangle, |0\rangle + i|1\rangle\}^{\otimes 2}$ and analyzed the output states. The experimentally reconstructed process matrix χ_{exp} is presented together with the ideal χ_{ideal} in Fig. 4. Using the definition of the process fidelity $F_p = [\text{Tr}(\sqrt{\sqrt{\chi_{\text{exp}}}\chi_{\text{ideal}}\sqrt{\chi_{\text{exp}}}})]^2$ [8], we obtained $F_p = 0.82 \pm 0.01$, which is at the same level as that in the previous works [7–9].

The progress we have made here is multifaceted. First, as new multimode photonic devices, the beam splitter and attenuator we developed can also be used as basic components for various optical information processing applications. Second, the CNOT gate we achieved is the first and indispensable demonstration of a 2-qubit logic gate with transverse mode encoding. Together with the single-qubit rotation operation realized previously [18,19], the CNOT gate makes universal quantum computation with transverse mode-encoded qubits possible. Compared to the chip size

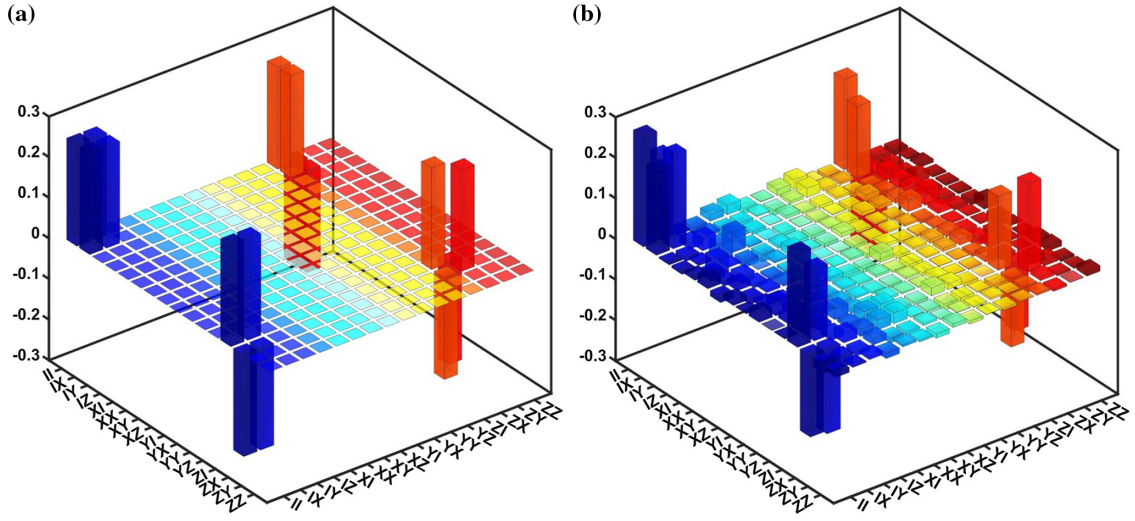

FIG. 4. Fig. 4. Quantum process tomography measurement results. Real parts of the density matrices for (a) an ideal controlled-NOT gate χ_{ideal} and (b) the measured χ_{exp}. The imaginary part of χ_{exp} is negligible. Here, $\boldsymbol{X}$, $\boldsymbol{Y}$, and Z represent the Pauli matrices σ_X, σ_Y, and σ_Z, respectively.

of path- and polarization-encoding CNOT gates based on dielectric waveguides (approximately 10^5–10^7 μm^2) [7–9], transverse mode encoding enables us to further shrink the chip size to approximately 10×160 μm^2 and improves chip stability when it becomes necessary to cascade multiple logic gates in large-scale photonic circuits. The gate is promising for high-dimensional quantum information applications by introducing more transverse modes. The gate is also compatible with the use of other d.o.f.s for encoding [18] and offers the possibility for diverse functions with hybrid encoding. Fully on-chip manipulation of transverse mode-encoded qubits is readily achievable with the integration of an entangled photon pair source using a multimode photonic waveguide [20]. It should be noted that the imperfect gate fidelity reported here is mainly due to the fabrication error, which resulted in additional insertion loss for higher-order transverse modes. The rapid development on nanofabrication technologies will definitely reduce these errors and thus improve the fidelity.

In conclusion, we have demonstrated the multimode implementation of a 2-qubit CNOT gate with transverse mode encoding, which consists of a newly developed multimode directional coupler and attenuator. The measured quantum state tomography shows that the entangled Bell states were generated by the gate operation with an average fidelity of $\bar{F}_s = 0.89 \pm 0.02$ and that quantum locality was violated by 10 standard deviations. Quantum process tomography was also performed to fully characterize the device, which exhibited a process fidelity of $F_p = 0.82 \pm 0.01$. The device is compact and extendable for higher dimensions, and it paves the way for on-chip quantum information processing with multiple d.o.f.s and higher capacity.

This work was supported by the National Natural Science Foundation of China (NSFC) (No. 61590932, No. 62005239, No. 11774333, No. 62061160487, No. 12004373, No. 91950205, No. 61961146003), National Science Fund for Distinguished Young Scholars (61725503), the Strategic Priority Research Program of the Chinese Academy of Sciences (No. XDB24030601), the National Key R & D Program (No. 2016YFA0301700), Anhui Initiative in Quantum Information Technologies (No. AHY130300), Zhejiang Provincial Natural Science Foundation (LZ18F050001, LD19F050001, LQ21F050006), the Postdoctoral Science Foundation of China (No. 2020M671860), and the Fundamental Research Funds for the Central Universities. This work was partially carried out at the USTC Centre for Micro and Nanoscale Research and Fabrication.

*These authors contributed equally to this work.
†dxdai@zju.edu.cn
‡renxf@ustc.edu.cn

[1] D. Dai, J. Wang, and Y. Shi, Silicon mode (de)multiplexer enabling high capacity photonic networks-on-chip with a single-wavelength-carrier light, Opt. Lett. **38**, 1422 (2013).
[2] J. Wang, S. Paesani, Y. Ding, R. Santagati, P. Skrzypczyk, A. Salavrakos, J. Tura, R. Augusiak, L. Mancinska, D. Bacco, D. Bonneau, J. W. Silverstone, Q. Gong, A. Acin, K. Rottwitt, L. K. Oxenlowe, J. L. O'Brien, A. Laing, and M. G. Thompson, Multidimensional quantum entanglement with large-scale integrated optics, Science **360**, 285 (2018).
[3] J. Wang, F. Sciarrino, A. Laing, and M. G. Thompson, Integrated photonic quantum technologies, Nat. Photonics **14**, 273 (2020).
[4] J. L. O'Brien, A. Furusawa, and J. Vučković, Photonic quantum technologies, Nat. Photonics **3**, 687 (2009).
[5] J. L. O'Brien, G. J. Pryde, A. G. White, T. C. Ralph, and D. Branning, Demonstration of an all-optical quantum controlled-NOT gate, Nature (London) **426**, 264 (2003).
[6] N. Kiesel, C. Schmid, U. Weber, R. Ursin, and H. Weinfurter, Linear Optics Controlled-Phase Gate Made Simple, Phys. Rev. Lett. **95**, 210505 (2005).
[7] A. Politi, M. J. Cryan, J. G. Rarity, S. Yu, and J. L. O'brien, Silica-on-silicon waveguide quantum circuits, Science **320**, 646 (2008).
[8] A. Crespi, R. Ramponi, R. Osellame, L. Sansoni, I. Bongioanni, F. Sciarrino, G. Vallone, and P. Mataloni, Integrated photonic quantum gates for polarization qubits, Nat. Commun. **2**, 566 (2011).
[9] P. J. Shadbolt, M. R. Verde, A. Peruzzo, A. Politi, A. Laing, M. Lobino, J. C. F. Matthews, M. G. Thompson, and J. L. O'Brien, Generating, manipulating and measuring entanglement and mixture with a reconfigurable photonic circuit, Nat. Photonics **6**, 45 (2012).
[10] P. C. Humphreys, B. J. Metcalf, J. B. Spring, M. Moore, X. Jin, M. Barbieri, W. S. Kolthammer, and I. A. Walmsley, Linear Optical Quantum Computing in a Single Spatial Mode, Phys. Rev. Lett. **111**, 150501 (2013).
[11] H. P. Lo, T. Ikuta, N. Matsuda, T. Honjo, W. J. Munro, and H. Takesue, Quantum Process Tomography of a Controlled-Phase Gate for Time-Bin Qubits, Phys. Rev. Applied **13**, 034013 (2020).
[12] H. H. Lu, J. M. Lukens, B. P. Williams, P. Imany, N. A. Peters, A. M. Weiner, and P. Lougovski, A controlled-NOT gate for frequency-bin qubits, npj Quantum Inf. **5**, 24 (2019).
[13] J. T. Barreiro, T. C. Wei, and P. G. Kwiat, Beating the channel capacity limit for linear photonic superdense coding, Nat. Phys. **4**, 282 (2008).
[14] X. L. Wang, X. D. Cai, Z. E. Su, M. C. Chen, D. Wu, L. Li, N. L. Liu, C. Y. Lu, and J. W. Pan, Quantum teleportation of multiple degrees of freedom of a single photon, Nature (London) **518**, 516 (2015).
[15] C. Li, D. Liu, and D. Dai, Multimode silicon photonics, Nanophotonics **8**, 227 (2019).
[16] L. W. Luo, N. Ophir, C. P. Chen, L. H. Gabrielli, C. B. Poitras, K. Bergmen, and M. Lipson, WDM-compatible mode-division multiplexing on a silicon chip, Nat. Commun. **5**, 3069 (2014).
[17] D. Dai, C. Li, S. Wang, H. Wu, Y. Shi, Z. Wu, S. Gao, T. Dai, H. Yu, and H. K. Tsang, 10-channel mode

(de) multiplexer with dual polarizations, Laser Photonics Rev. **12**, 1700109 (2018).
[18] L. T. Feng, M. Zhang, Z. Y. Zhou, M. Li, X. Xiong, L. Yu, B. S. Shi, G. P. Guo, D. X. Dai, X. F. Ren, and G. C. Guo, On-chip coherent conversion of photonic quantum entanglement between different degrees of freedom, Nat. Commun. **7**, 11985 (2016).
[19] A. Mohanty, M. Zhang, A. Dutt, S. Ramelow, P. Nussenzveig, and M. Lipson, Quantum interference between transverse spatial waveguide modes, Nat. Commun. **8**, 14010 (2017).
[20] L. T. Feng, M. Zhang, X. Xiong, Y. Chen, H. Wu, M. Li, G. P. Guo, G. C. Guo, D. X. Dai, and X. F. Ren, On-chip transverse-mode entangled photon pair source, npj Quantum Inf. **5**, 2 (2019).
[21] S. Paesani, M. Borghi, S. Signorini, A. Maïnos, L. Pavesi, and A. Laing, Near-ideal spontaneous photon sources in silicon quantum photonics, Nat. Commun. **11**, 2505 (2020).
[22] C. Wang, X. Xiong, N. Andrade, V. Venkataraman, X. F. Ren, G. C. Guo, and M. Lončar, Second harmonic generation in nano-structured thin-film lithium niobate waveguides, Opt. Express **25**, 6963 (2017).
[23] E. A. Kittlaus, N. T. Otterstrom, and P. T. Rakich, On-chip inter-modal Brillouin scattering, Nat. Commun. **8**, 15819 (2017).
[24] Y. Ding, J. Xu, F. D. Ros, B. Huang, H. Ou, and C. Peucheret, On-chip two-mode division multiplexing using tapered directional coupler-based mode multiplexer and demultiplexer, Opt. Express **21**, 10376 (2013).
[25] J. Wang, P. Chen, S. Chen, Y. Shi, and D. Dai, Improved 8-channel silicon mode demultiplexer, Opt. Express **22**, 12799 (2014).
[26] Y. Lai, Y. Yu, S. Fu, J. Xu, P. P. Shum, and X. Zhang, Compact double-part grating coupler for higher-order mode coupling, Opt. Lett. **43**, 3172 (2018).
[27] B. Stern, X. Zhu, C. P. Chen, L. D. Tzuang, J. Cardenas, K. Bergman, and M. Lipson, On-chip mode-division multiplexing switch, Optica **2**, 530 (2015).
[28] H. Jia, T. Zhou, L. Zhang, J. Ding, X. Fu, and L. Yang, Optical switch compatible with wavelength division multiplexing and mode division multiplexing for photonic networks-on-chip, Opt. Express **25**, 20698 (2017).
[29] Y. Xiong, R. Priti, and O. Ladouceur, High-speed two-mode switch for mode-division multiplexing optical networks, Optica **4**, 1098 (2017).
[30] Q. Huang, K. Jie, Q. Liu, Y. Huang, Y. Wang, and J. Xia, Ultra-compact, broadband tunable optical bandstop filters based on a multimode one-dimensional photonic crystal waveguide, Opt. Express **24**, 20542 (2016).
[31] Y. Liu, K. Xu, S. Wang, W. Shen, H. Xie, Y. Wang, S. Xiao, Y. Yao, J. Du, Z. He, and Q. Song, Arbitrarily routed mode-division multiplexed photonic circuits for dense integration, Nat. Commun. **10**, 3263 (2019).
[32] S. Li, Y. Zhou, J. Dong, X. Zhang, E. Cassan, J. Hou, C. Yang, S. Chen, D. Gao, and H. Chen, Universal multimode waveguide crossing based on transformation optics, Optica **5**, 1549 (2018).
[33] D. Dai, W. Zhao, J. Guo, and D. Liu, Multimode silicon photonic devices, Integr. Opt. **11689**, 116890N (2021).
[34] M. Nielsen and I. Chuang, *Quantum Computation and Quantum Information* (Cambridge University Press, Cambridge, England, 2000).
[35] C. K. Hong, Z. Y. Ou, and L. Mandel, Measurement of Subpicosecond Time Intervals between Two Photons by Interference, Phys. Rev. Lett. **59**, 2044 (1987).
[36] W. Bogaerts, R. Baets, P. Dumon, V. Wiaux, S. Beckx, D. Taillaert, B. Luyssaert, J. V. Campenhout, P. Bienstman, and D. V. Thourhout, Nanophotonic waveguides in silicon-on-insulator fabricated with CMOS technology, J. Lightwave Technol. **23**, 401 (2005).
[37] See Supplemental Material at http://link.aps.org/supplemental/10.1103/PhysRevLett.128.060501 for more details about characterization of passive structures, analysis of quantum states and experimental setups.
[38] E. Knill, R. Laflamme, and G. J. Milburn, A scheme for efficient quantum computation with linear optics, Nature (London) **409**, 46 (2001).
[39] D. F. V. James, P. G. Kwiat, W. J. Munro, and A. G. White, Measurement of qubits, Phys. Rev. A **64**, 052312 (2001).
[40] T. C. Wei, K. Nemoto, P. M. Goldbart, P. G. Kwiat, W. J. Munro, and F. Verstraete, Maximal entanglement versus entropy for mixed quantum states, Phys. Rev. A **67**, 022110 (2003).
[41] V. Coffman, J. Kundu, and W. K. Wootters, Distributed entanglement, Phys. Rev. A **61**, 052306 (2000).
[42] J. F. Clauser, M. A. Horne, A. Shimony, and R. A. Holt, Proposed Experiment to Test Local Hidden-Variable Theories, Phys. Rev. Lett. **23**, 880 (1969).